

Article

# Optical Coherence Tomography Reveals Sigmoidal Crystalline Lens Changes during Accommodation

George A. Gibson, Fiona E. Cruickshank , James S. Wolffsohn and Leon N. Davies \*

Ophthalmic Research Group, Life and Health Sciences, Aston University, Birmingham B4 7ET, UK; tony.gibson@college-optometrists.org (G.A.G.); f.cruickshank@aston.ac.uk (F.E.C.); j.s.w.wolffsohn@aston.ac.uk (J.S.W.)

\* Correspondence: l.n.davies@aston.ac.uk; Tel.: +44-(0)121-204-4152

Received: 20 July 2018; Accepted: 17 August 2018; Published: 21 August 2018



**Abstract:** This study aimed to quantify biometric modifications of the anterior segment (AS) during accommodation and to compare them against changes in both accommodative demand and response. Thirty adults, aged 18–25 years were rendered functionally emmetropic with contact lenses. AS optical coherence tomography (AS-OCT) images were captured along the 180° meridian (Visante, Zeiss Meditec, Jena, Germany) under stimulated accommodative demands (0–4 D). Images were analysed and lens thickness (LT) was measured, applying a refractive index correction of 1.00. Accommodative responses were also measured sequentially through a Badal optical system fitted to an autorefractor (Shin Nippon NVision-K 5001, Rexxam, Japan). Data were compared with Dubbelman schematic eye calculations. Significant changes occurred in LT, anterior chamber depth (ACD), lens centroid (i.e.,  $ACD + LT/2$ ), and AS length ( $ASL = ACD + LT$ ) with accommodation (all  $p < 0.01$ ). There was no significant change in CT with accommodation ( $p = 0.81$ ). Measured CT, ACD, and lens centroid values were similar to Dubbelman modelled parameters, however AS-OCT overestimated LT and ASL. As expected, the accommodative response was less than the demand. Interestingly, up until approximately 1.5 D of response (2.0 D demand), the anterior crystalline lens surface appears to be the primary correlate. Beyond this point, the posterior lens surface moves posteriorly resulting in an over-all sigmoidal trajectory. The posterior crystalline lens surface demonstrates a sigmoidal response with increasing accommodative effort.

**Keywords:** accommodation; crystalline lens; imaging; in-vivo; optical coherence tomography

## 1. Introduction

Accommodative refractive change is primarily brought about by alterations in the surface curvatures of the crystalline lens. During accommodation, the anterior radius of curvature decreases [1–3], accompanied by a smaller simultaneous steepening of the posterior surface [4–6]. The lens equatorial diameter decreases [7–15], with the associated curvature changes resulting in a reduction of the anterior chamber depth [1,16–22] and an increase in lens axial thickness [1,5,16–21,23–27]. Crystalline lens surface curvature changes are the primary cause of dioptric change with accommodation [3,19]. Alterations in axial surface distances (i.e., the reduction in anterior chamber depth (ACD) and increase in crystalline lens thickness (LT)) appear to reduce accommodative response with increasing levels of accommodative demand [5,28].

A number of different methods have been employed to quantify intraocular surface distances. A-scan ultrasonography has been used to measure static changes in ocular biometry in humans and primates, the latter using Edinger-Westphal (EW) and pharmacological stimulation [1,29–33]. Dynamic changes in anterior segment (AS) biometry have also been studied in humans and primates using continuous high-resolution ultrasonography [9,20,29,33–43]. Other imaging techniques are

also capable of quantifying ocular biometric changes associated with accommodation. These include Scheimpflug photography [1,2,19,44–47], magnetic resonance imaging (MRI) [8,12,24], partial coherence interferometry (PCI) [17,21,48], and AS optical coherence tomography (AS-OCT) [26,49–51]. Hitherto, AS-OCT has been used to measure anterior chamber depth, width and angle [49,52–57], to evaluate phakic intraocular lens implants [58–60] and to determine corneal integrity [61–63]. The accuracy of this ocular biometric data is also important in determining the risk of angle closure glaucoma, and for pre- and post-operative assessment in cataract and kerato-refractive surgery [53].

AS-OCT also allows measurement of ocular biometric changes associated with the accommodative response. Richdale et al. [26] showed that lens thickness changes during accommodation as measured with the Visante AS-OCT (Carl Zeiss Meditec, Dublin, CA, USA) are comparable to previous findings using Scheimpflug photography [18], ultrasound [4], MRI [12] and PCI [21,64]. However, a limitation of this work is that biometric alterations have been plotted against accommodative stimulus and not response [26], which may have led to erroneous conclusions. Hence, this study aims to quantify AS changes during accommodation in a cohort of young participants. Importantly, and in contrast to previous work, biometric modifications are compared against changes in both accommodative demand and response. In addition, comparisons are made with data from a well-validated schematic model eye [65] based on empirical work acquired with Scheimpflug photography [45–47]. A mean age of 19.4 years has been used for Dubbelman values.

## 2. Materials and Methods

Thirty participants from Aston University were recruited, aged 18 to 25 years (mean  $\pm$  SD,  $19.4 \pm 2.0$  years) 40% of whom were male. Mean spherical equivalent (MSE; sphere + [cylinder/2]) was  $-1.85 \text{ D} \pm 2.68 \text{ D}$  (range:  $+1.94 \text{ D}$  to  $-6.87 \text{ D}$ ). Participants with astigmatism  $\geq 1.0 \text{ D}$  were excluded from the study. All participants achieved 0.0 logMAR visual acuity or better in the eye tested, with a subjective amplitude of accommodation  $\geq 8.0 \text{ D}$  (RAF gauge, Clement Clarke/Haag-Streit, Harlow, UK). No participant had any form of visual or pathological anomaly. Participants were furnished with a full explanation of the procedures involved in the investigation, and gave informed consent to their participation, in line with the tenets of the Declaration of Helsinki. Ethical approval was granted by the Human Ethics Committee of Aston University.

Uncorrected distance autorefractometry was performed on each participant using the previously validated Shin-Nippon *NVision-K 5001* (Shin-Nippon Commerce Inc., Tokyo, Japan) open view autorefractor [66]. Slit lamp examination was performed on all participants to assess anterior eye health and suitability for contact lens wear, before participants were rendered functionally emmetropic with conventional daily disposable spherical soft contact lenses (etafilcon A, 58% water content, Johnson & Johnson Vision, Jacksonville, FL, USA) to ensure that the accommodative demand was virtually identical for each subject. Sufficient time (approximately 15 min) was given for adaptation to the soft contact lenses before assessment. All participants were existing soft contact lens wearers, and no participant experienced difficulties. All participants were experienced with visual experiments and, prior to the full study, were trained to maintain steady fixation.

Initially, the residual refractive error of each participant was measured whilst viewing a Maltese cross (contrast: 78%; luminance:  $32 \text{ cdm}^{-2}$ ) through a  $+5.0 \text{ D}$  Badal optical system with the target placed at  $0.0 \text{ D}$ . Participants were excluded if their MSE residual refractive error exceeded  $\pm 0.25 \text{ D}$ , or if the residual cylindrical component was  $>0.50 \text{ DC}$ . With the left eye occluded, the right eye of each participant viewed the stationary Maltese cross target through the Badal optical system, fitted to the autorefractor. Five accommodative stimulus levels were presented in a random order within the Badal system ( $0.0 \text{ D}$  to  $4.0 \text{ D}$  in  $1.0 \text{ D}$  steps). Participants were encouraged to “carefully focus” [67] on the target at all times, as attentional factors can influence accommodation measurement [68]. Five measures of the participant’s accommodation response were recorded at each stimulus level and averaged to provide a stimulus-response profile.

To measure the associated biometric changes in crystalline lens thickness and position, participants were asked to place their head on the automated chin and headrest of the AS-OCT (Visante OCT, model 1000, Carl Zeiss Meditec, Dublin, CA, USA) so that the captured image of the eye was central in the integral computer monitor window. Again, participants were encouraged to concentrate on the internal pinwheel target at all times. Two separate images were captured along the 180° meridian in the AS single-image capture mode. According to the instrument's user manual, this setting provides an axial resolution of approximately 18 µm and a transverse resolution of 60 µm with an axial scan accuracy of ±15 µm (1 SD) over 6 mm. The device employs low-coherence interferometry, via a superluminescent light-emitting diode (central wavelength 1310 nm, optical power <6.5 mW at the cornea). The scanning spot moves rapidly across the eye, acquiring 2000 A-scans per second, with a scan time of 0.125 s per line in anterior segment mode, to generate a two-dimensional image which covers an area of 16 mm in width and 6 mm in depth.

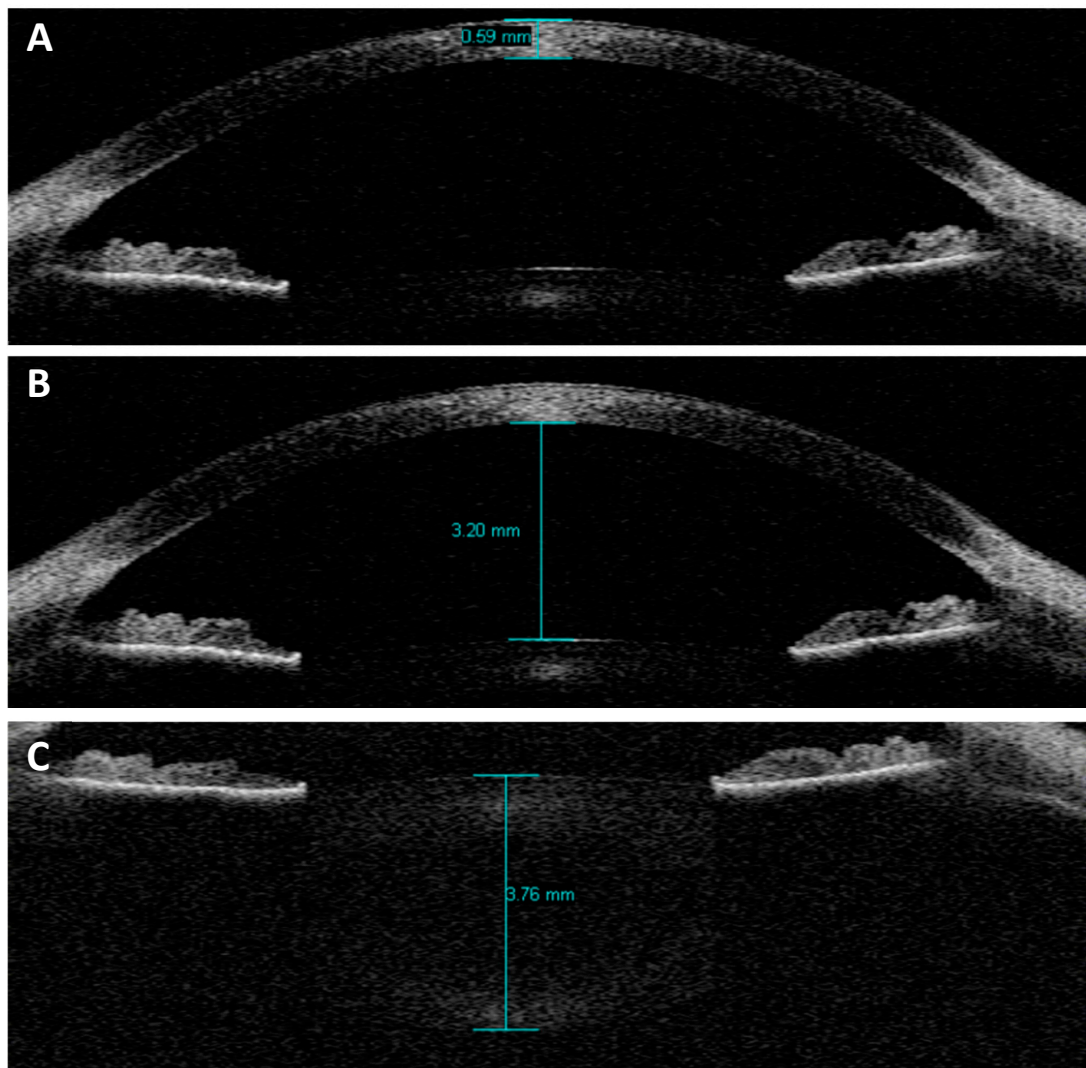
The first image included corneal thickness and anterior chamber depth (Figure 1A,B respectively). The second image involved changing the focal plane of the AS-OCT, enabling measurement of crystalline lens thickness (Figure 1C). As with the autorefractor measures, participants were exposed to five stimulus levels, presented in a random order, using the AS-OCT's internal pinwheel target and the internal adjustable Badal lens system. This process was repeated three times to generate mean AS changes.

Image analysis was performed using the Visante's built-in software (version 1.0.12.1896, Carl Zeiss Meditec, Dublin, CA, USA). The software has an inbuilt refractive indices adjustment feature which uses edge detection algorithms to locate corneal surfaces and automatically assign appropriate indices to each region of the image and, therefore, automatically scale individual structural dimensions [69]. A refractive index of 1.00 (air) is applied to the region anterior to the cornea, 1.338 (cornea) for the region within the corneal boundaries, and 1.343 (aqueous humour) for structures posterior to the cornea. However, when imaging the crystalline lens, the cornea is not simultaneously visible; therefore, appropriate dimensional adjustments cannot be made. Consequently, a refractive index of 1.00 was applied to the entirety of all images using the Edit Surfaces option, before measurements were taken, as in previous studies that have examined internal ocular structures without a simultaneous corneal image [69].

All images were analysed by the same examiner (G.A.G.). Following refractive index adjustment, intraocular distances were measured using the built-in Visante measuring calipers. Measurement involved the manual placement of the endpoint of each caliper arm on the boundary edge of the relevant anterior segment structural landmark. Corneal thickness (CT) was defined as the anteroposterior distance between the cornea's front-most and back-most surfaces (Figure 1A), anterior chamber depth (ACD) as the distance between the posterior corneal surface and the anterior crystalline lens surface (Figure 1B) and lens thickness (LT) as the distance between the anterior crystalline lens surface and the posterior crystalline lens surface (Figure 1C). Where necessary, adjustments to brightness and contrast settings were made using the software's built-in capabilities, to facilitate localisation of the relevant structural boundaries. Furthermore, the software allows the operator to manually adjust the image magnification to enhance the accuracy of caliper placement. Lens centroid ( $LC = ACD + LT/2$ ) and anterior segment length ( $ASL = ACD + LT$ ; the position of the posterior crystalline lens surface) were then calculated from ACD and LT measures. All distances were measured three separate times. Means and standard deviations were calculated using a Microsoft Excel spreadsheet.

The Dubbelman eye model is a schematic eye derived by Norrby [65], and is based on the work of Dubbelman and colleagues, who collected substantial biometric data using Scheimpflug photography [45–47]. The model incorporates aspheric surfaces and can be used to compute predicted intraocular biometric dimensions and spacings. Equations were based on the same group of 102 eyes in which the mean refractive error was −1.10 D, including 42 myopes, 47 near emmetropes and 13 hyperopes. Participants were aged 16–65 years (mean 39.2 years) [45–47]. The Dubbelman Eye

Model has been chosen to validate the crystalline lens measures in the current study, as it can be altered for both age (A) and accommodation demand (D) (as all of the studies used to derive the Model were based on accommodative demand rather than accommodative response). Refractive parameters and the formulae used to derive biometrics from the Dubbelman eye model are shown in Table 1. For the current study, values for CT, ACD, and LT were calculated from these formulae with an inputted age (A) of 19.4 years to match the average age of the participant cohort. Calculations were performed at accommodation levels of 0.00 to 4.00 dioptres in steps of 1.0 D to provide a modelled value to match the data for each stimulus level collected from the participants. LC and ASL values were calculated from the ACD and LT values modelled for the same stimulus level, using the same equations as used for participant data.



**Figure 1.** The Visante AS-OCT screen displaying measuring calipers in situ for measurement of (A) corneal thickness (CT), (B) anterior chamber depth (ACD) and (C) lens thickness (LT). Images are not shown for anterior segment length (ASL) or lens centroid (LC) as these values are derived by calculation from CT, ACD, and LT measures. Note that though CT and ACD are drawn on separate images here for demonstration purposes, during real data analysis calipers were drawn simultaneously on the same image using the software's function to hide from view calipers which obscure the region required for subsequent measures.

Statistical Analysis

A repeated measures analysis of variance (ANOVA) [70] was conducted with SPSS 12.0.1 for Microsoft Windows (SPSS Inc, Chicago, IL, USA), where accommodation demand was taken as the within-subject variable. A sample size calculation using G\*Power 3 [71] was based on a repeated measures ANOVA, with an effect size (f) of 0.25, an error probability ( $\alpha$ ) of 0.05, and required power ( $1 - \beta$ ) of 0.90 for five repeated measurements, indicated 26 participants were required.

**Table 1.** The Dubbelman eye model [65]. Component radii, axial thicknesses, and refractive indices are shown. The equations shown refer to the dependence of various components on years of age (A) and dioptries of accommodative demand (D).

Component	Parameter
Cornea	
Anterior radius (mm)	7.87
Thickness (mm)	0.574
Refractive index	1.376
Posterior radius (mm)	6.40
Anterior Chamber	
Depth (mm)	$3.87 - 0.010A - D$ (0.048 – 0.0004A)
Refractive index	1.336
Crystalline Lens	
Anterior radius (mm)	$1/[1/(12.7 - 0.058A) + 0.0077D]$
Thickness (mm)	$2.93 + 0.0236A + D$ (0.058 – 0.0005A)
Refractive index	$1.441 - 0.00039A + 0.0013D$
Posterior radius (mm)	$1/[1/(5.9 - 0.0013A) + 0.0043D]$
Vitreous	
Depth (mm)	Variable (see text)
Refractive index	1.376

3. Results

The mean magnitude of change during accommodation as measured by the AS-OCT was similar to the Dubbleman eye model [65]. Moreover, the measures for CT, ACD, LT, LC, and ASL were also similar (Table 2). The largest discrepancy between approaches appears to be LT and ASL, where the AS-OCT appears to overestimate these components in comparison to the Scheimpflug data described by Dubbelman [19,45–47].

Some studies [5,21,49], which have assessed AS biometric changes, consider the ACD to be the distance between the anterior vertex of the cornea and the anterior vertex of the crystalline lens, thus including the thickness of the cornea. The absolute values displayed in Table 2, therefore, require the addition of the corneal thickness to allow comparisons to be made across studies. For example, the mean ACD of the Dubbelman model at rest (0.0 D stimulus) is 3.67 mm. A similar calculation must be made when considering LC and ASL; these corrected data are also shown in Table 2.

As the studies by Dubbelman and colleagues rely on measures attributed to accommodative demand [19,45–47], a degree of error may be inherent in the model, as the axial distances and relative changes given may be related to a different accommodative response. Figure 2 illustrates, as expected, the accommodative response is less than that of demand, due to the lag of accommodation. What is also of interest is that the lens changes appear to be sigmoidal. Up until approximately 1.5 D of response (approximately 2.0 D demand), the anterior crystalline lens surface appears to be the primary correlate. After this point, the posterior surface begins to alter position. This is contrary to the model data (Figure 2C), which predict a linear pattern of lens changes.

**Table 2.** Anterior eye axial distances and their variation with accommodation demand measured with the AS-OCT, compared to the Dubbelman model eye data [65]. The average age of the cohort has been matched to that of the model (19.4 years old;  $n = 30$ ). The ACD and subsequent measures have been altered to include the corneal thickness where required. To note, correction for CT is not required for measures of LT alone.

Accommodation Demand (D)	Dubbelman Model (mm)	Dubbelman Model (mm) Adjusted for CT	AS-OCT (mm $\pm$ SD)	AS-OCT (mm $\pm$ SD) Adjusted for CT
Corneal Thickness (CT)				
0	0.574	-	0.551 $\pm$ 0.030	-
1	0.574	-	0.552 $\pm$ 0.033	-
2	0.574	-	0.553 $\pm$ 0.029	-
3	0.574	-	0.554 $\pm$ 0.029	-
4	0.574	-	0.552 $\pm$ 0.033	-
Anterior Chamber Depth (ACD)				
0	3.096	3.670	3.102 $\pm$ 0.280	3.653 $\pm$ 0.277
1	3.056	3.630	3.066 $\pm$ 0.287	3.618 $\pm$ 0.285
2	3.016	3.590	3.021 $\pm$ 0.287	3.574 $\pm$ 0.286
3	2.976	3.550	2.970 $\pm$ 0.283	3.524 $\pm$ 0.278
4	2.936	3.510	2.928 $\pm$ 0.282	3.480 $\pm$ 0.280
Lens Thickness (LT)				
0	3.402	-	3.632 $\pm$ 0.205	-
1	3.450	-	3.669 $\pm$ 0.200	-
2	3.498	-	3.719 $\pm$ 0.210	-
3	3.546	-	3.802 $\pm$ 0.226	-
4	3.594	-	3.867 $\pm$ 0.219	-
Lens Centroid (ACD + LT/2)				
0	4.797	5.371	4.918 $\pm$ 0.235	5.469 $\pm$ 0.232
1	4.781	5.355	4.900 $\pm$ 0.235	5.452 $\pm$ 0.233
2	4.765	5.339	4.881 $\pm$ 0.239	5.434 $\pm$ 0.237
3	4.749	5.323	4.871 $\pm$ 0.232	5.425 $\pm$ 0.229
4	4.733	5.307	4.861 $\pm$ 0.228	5.413 $\pm$ 0.226
Anterior segment Length (ACD + LT)				
0	6.498	7.072	6.734 $\pm$ 0.230	7.285 $\pm$ 0.229
1	6.506	7.080	6.735 $\pm$ 0.220	7.287 $\pm$ 0.218
2	6.514	7.088	6.740 $\pm$ 0.231	7.294 $\pm$ 0.230
3	6.522	7.096	6.772 $\pm$ 0.232	7.326 $\pm$ 0.231
4	6.530	7.104	6.795 $\pm$ 0.221	7.347 $\pm$ 0.218

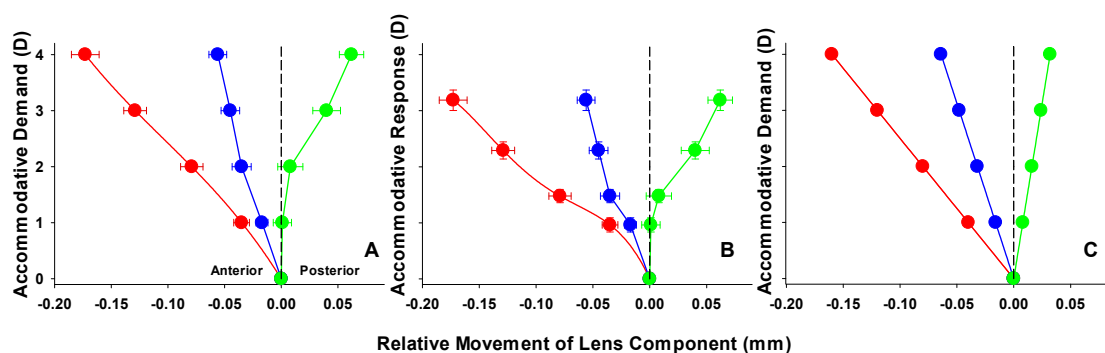


**Figure 2.** Relative movements of the various lens parameters as a function of accommodative demand or response. Red markers represent the anterior lens surface, blue markers the lens centroid and green markers the posterior lens surface. (A) The relative movement of the lens components for the AS-OCT data with accommodative demand (error bars represent  $\pm$ SEM). (B) The relative movement of the lens components for the AS-OCT data with accommodative response ( $\pm$ SEM). (C) The relative movement of the lens components for the Dubbelman model eye [65] with accommodative demand.

When comparing the relative changes in axial distances, the two methods (Scheimpflug and AS-OCT) appear to be more closely associated (Table 3). These axial measures are very similar, with the AS-OCT data falling very close to the model distances. Corneal thickness did not change with accommodation ( $F_{(4,29)} = 0.40; p = 0.81$ ). All other measures, however, reached statistical significance (ACD:  $F_{(4,29)} = 116.96; p < 0.01$ , LT:  $F_{(4,29)} = 128.97; p < 0.01$ , LC:  $F_{(4,29)} = 17.30; p < 0.01$ , ASL:  $F_{(4,29)} = 13.67; p < 0.01$ ). When the AS-OCT distances were corrected to include CT, the accommodative changes remained significant (ACD:  $F_{(4,29)} = 117.56; p < 0.01$ , LC:  $F_{(4,29)} = 17.45; p < 0.01$ , ASL:  $F_{(4,29)} = 14.72; p < 0.01$ ).

**Table 3.** Anterior eye relative axial distance changes with accommodation demand measured with the AS-OCT, compared to the Dubbelman model eye data [65]. The average age of the cohort has been matched to that of the model (19.4 years old;  $n = 30$ ).

Accommodation Demand (D)	Dubbelman Model (mm)	AS-OCT (mm ± SD)
Anterior chamber depth (ACD)		
1	−0.040	−0.035 ± 0.038
2	−0.080	−0.079 ± 0.054
3	−0.120	−0.129 ± 0.055
4	−0.160	−0.173 ± 0.067
Lens Thickness (LT)		
1	0.048	0.037 ± 0.059
2	0.096	0.087 ± 0.070
3	0.144	0.170 ± 0.083
4	0.192	0.235 ± 0.091
Lens Centroid (ACD + LT/2)		
1	−0.016	−0.017 ± 0.029
2	−0.032	−0.035 ± 0.046
3	−0.048	−0.045 ± 0.045
4	−0.064	−0.056 ± 0.043
Anterior segment Length (ACD + LT)		
1	0.008	0.001 ± 0.044
2	0.016	0.008 ± 0.061
3	0.024	0.040 ± 0.067
4	0.032	0.062 ± 0.059

#### 4. Discussion

Understanding the changes in anterior segment geometry with accommodation is critical to understanding fully the lenticular mechanism of accommodation. AS-OCT is an important technological advance, which has provided a non-invasive means of accurately visualising the performance and morphology of the accommodative apparatus and its associated biometric modifications in vivo. As such, some of the uncertainties previously attributed to the difficulties of obtaining direct measures of the accommodative apparatus' elements as they work in concert are now being illuminated. However, a limitation of some previous work is a tendency to consider biometric modifications in terms of accommodative demand in isolation, rather than a measured response. This study provides estimates of the ocular biometry associated with accommodation in the adult human eye, with reference to both accommodative demand and response and, furthermore, compares them with those predicted from accommodating model eye calculations [65].

The key accommodative changes in anterior segment biometry in the present investigation are a reduction in ACD, an increase in LT, a reduction in LC, and an increase in ASL, while corneal thickness was unchanged (Table 2), all consistent with the Helmholtzian model of accommodation. In the accommodated state (4 D stimulus) LT increased by 0.24 mm compared to in the unaccommodated state, consistent with previous reports [1,5,16–21,23–27], while there was a concurrent 0.06 mm reduction in lens centroid and 0.061 mm increase in ASL. Furthermore, this study reports agreement

between axial separations measured on AS-OCT images, and those predicted from accommodating model eye calculations [65]. However, the lens thickness and, subsequently, ASL values appear to be overestimated by AS-OCT compared to the calculated figures (Table 3); a finding which is corroborated by the work of Dunne and colleagues [72].

Measured ACD was significantly shallower (0.17 mm) in the unaccommodated state compared to under 4.00 D of accommodative stimulus, in accordance with previous *in vivo* reports [1,16–22]. Baikoff et al. [49] found a mean reduction in ACD length of  $30 \mu\text{mD}^{-1}$  using AS-OCT, comparable to the present study's measured and modelled values of  $34 \mu\text{mD}^{-1}$  and  $40 \mu\text{mD}^{-1}$ , respectively. Ostrin et al. [20] found this decrease to be greater, in the region of  $51 \mu\text{mD}^{-1}$  using A Scan and a young cohort of between 21 and 30 years, whereas Bolz et al. [64] found a decrease of  $47 \mu\text{mD}^{-1}$  in emmetropes and  $57 \mu\text{mD}^{-1}$  in myopes using PCI.

The current study reports a  $58 \mu\text{mD}^{-1}$  rate of change in LT with accommodation, comparable to the work of Richdale and colleagues [26] who found a  $51 \mu\text{mD}^{-1}$  increase, also using AS-OCT. The results from both studies are greater than those predicted by the Dubbelmann model ( $45 \mu\text{mD}^{-1}$ ). Other studies, which have determined LT based on PCI, have found variable thickness changes, in the order of  $36 \mu\text{mD}^{-1}$  [21], and in a separate study,  $63 \mu\text{mD}^{-1}$  for emmetropes and  $72 \mu\text{mD}^{-1}$  for myopes [64]. An ultrasound study has reported a lower value of  $42 \mu\text{mD}^{-1}$  [4]. It must be stressed that the stimuli used these studies inevitably vary with instrumentation and study group. Alterations in axial surface distances (i.e., the reduction in anterior chamber depth (ACD) and the increase in crystalline lens thickness (LT)) appear to reduce accommodative response with increasing levels of accommodative demand [5,28].

Perhaps the most interesting and novel finding of this study is the sigmoidal response of the posterior crystalline lens surface during accommodation; a phenomenon so far unreported in the literature, with previous human and animal studies finding an equal and linear change in the anterior and posterior portions of the lens with accommodation [1,29]. In the current study, the posterior surface appears to be relatively static until approximately 1.5 D of response (approximately 2.0 D demand), after which it begins to make its posterior motion (Figure 2B). Drexler and colleagues [17] plotted the position of the anterior and posterior poles of the crystalline lens with change in fixation from far viewing to targets at various closer distances. The results show a static posterior lens surface from distance observation until viewing a target at 40.0 cm (2.5 D stimulus). From this point, closer targets elicit a posterior movement of the surface of just over 0.5 mm for a target at 10.0 cm (10.0 D stimulus); this phenomenon is, however, not alluded to in the text; it appears to be relatively new in the study of accommodative lenticular changes. What is well established from other work is that the changes in lenticular radius during accommodation are greater for the anterior surface of the lens [1–3,5]. The initial absence of movement of the posterior lens surface to low accommodative stimuli, may, perhaps result from a mechanical resistance exerted by the vitreous body. In combination with the forward movement of the anterior lens surface, there is a resulting increase in axial thickness and a small forward movement of the LC [17,23,24]. This may also explain why there is a similar, though much less pronounced sigmoidal response also seen for the anterior lens surface, potentially due to a similar resistance to forward movement by the aqueous humour. The relatively lower magnitude of the initial inertia may be due to the relatively smaller volume of humour against the lens' anterior face and therefore less mechanical restriction. It is known that the vitreous body undergoes a syneresis with age [73], and therefore, it could be hypothesised that the posterior surface sigmoidal response may undergo attenuation with age as vitreous resistance lessens due to liquefaction. This again may have contributed a lack of sigmoidal response in the Dubbleman data and other such studies which have older or wide age inclusion criteria. It can be seen from our data that the shape of the measured functions are noticeably different between demand and response for anterior lens surface, posterior lens surface and lens centroid (Figure 2). Though the sigmoidal response can still be inferred from demand data, it is markedly less pronounced than shown for response. It may follow that



biometric studies which fail to consider accommodative responses may undergo a masking of such accommodative trends.

The findings of the current study notwithstanding, AS-OCT imaging does have some important limitations which are relevant to this study. Firstly, as with other two-dimensional imaging techniques [8], it is difficult to ensure that sequential AS-OCT slices are taken from the same plane. To mitigate this, the patient's forehead was in contact with the forehead rest at all times, and multiple images were acquired and averaged for each accommodative level. A further potential limitation associated with referencing an appropriate image slice plane concerns the putative cyclotorsion effects observed during accommodation [74] although this remains equivocal [75]. Although the Visante allows variation in the meridian of the image slice, this is only in one degree steps, which is insufficient to compensate for the small amounts of cyclotorsion associated with accommodation where mean cyclotorsion has been reported as  $0.62 \pm 2.18$  degrees excyclorotation for an accommodative stimulus up to 6.0 D [74].

Lack of image correction for optical and instrument distortion may also be of importance. The application of a standard refractive index (1.00) across both AS-OCT images was a necessary adjustment to ensure the comparability of within subject biometric measures. However, other studies using OCT imaging have utilized a system wherein separately collected corneal and lenticular images can be merged and corrected after capture [15,76]. The use of such a technique was not possible in the current study owing to the use of commercial, non-custom analysis software. Furthermore, the Visante, like other optical imaging techniques, assumes a single refractive index of the lens [12,26] (i.e., 1.42 [77,78]) and does not take into account the gradient refractive index (GRIN) of the crystalline lens as reported by other authors [12,45,76]. Studies have also specifically examined the correction of the posterior surface with different homogeneous refractive indices, and also using a GRIN [79,80], and have reported that for both thickness and shape measurement the best approach was to use an average refractive index ( $n = 1.408 \pm 0.005$ ) as defined by Uhlhorn and colleagues [81]. Though the precise effect of not applying such a correction factor on the accuracy of the present study is unknown, relative changes in axial separation of the ocular components were compared on the assumption that any distortion or manipulation of the image by the AS-OCT is constant throughout the image taken, thereby allowing comparison with other techniques. In this instance, the data points from the OCT and from the model eye are very close, with all model data falling well within the compass of any errors (SD) from the AS-OCT cohort.

## 5. Conclusions

The study reveals a sigmoidal response of the posterior lenticular surface with increasing accommodative effort; a phenomenon which has hitherto gone unreported in previous studies. Additionally, the use of axial distance measures acquired directly by AS-OCT compares well with a published schematic eye model [65]. Despite this, some caution should be taken when applying such linear models to infer the biometric corollaries of low accommodative stimuli, as they may not entirely reflect the true nature of the behaviour of the ocular structures. The majority of studies of this type relate biometric changes to the accommodative stimulus as opposed to the response. Although it is difficult to inextricably link accommodative demand and response, the latter would suggest a better evaluation of actual accommodative performance.

**Author Contributions:** Conceptualization, L.N.D.; Methodology, G.A.G., J.S.W., and L.N.D.; Software, G.A.G.; Formal Analysis, G.A.G., F.E.C., and L.N.D.; Investigation, G.A.G., J.S.W., and L.N.D.; Resources, J.S.W. and L.N.D.; Data Curation, G.A.G.; Writing—Original Draft Preparation, G.A.G.; Writing—Review and Editing, F.E.C., J.S.W., and L.N.D.; Visualization, F.E.C.; Supervision, J.S.W. and L.N.D.; Project Administration, L.N.D.; Funding Acquisition, L.N.D.

**Funding:** G.A.G. was funded by a Co-operative Award in Science and Engineering (CASE/CNA/05/51) from the Engineering and Physical Sciences Research Council (EPSRC) and Bausch and Lomb. F.E.C was funded by the College of Optometrists.

**Acknowledgments:** The study was presented, in part, at the 2009 ARVO annual meeting in Fort Lauderdale, FL, USA.

**Conflicts of Interest:** The authors have no financial or proprietary interest in any product, method, or material described in the manuscript.

## References

1. Koretz, J.F.; Cook, C.A.; Kaufman, P.L. Accommodation and presbyopia in the human eye. Changes in the anterior segment and crystalline lens with focus. *Investig. Ophthalmol. Vis. Sci.* **1997**, *38*, 569–578.
2. Koretz, J.F.; Cook, C.A.; Kaufman, P.L. Aging of the human lens: Changes in lens shape upon accommodation and with accommodative loss. *J. Opt. Soc. Am. A Opt. Image Sci. Vis.* **2002**, *19*, 144–151. [[CrossRef](#)] [[PubMed](#)]
3. Rosales, P.; Dubbelman, M.; Marcos, S.; van der Heijde, R. Crystalline lens radii of curvature from Purkinje and Scheimpflug imaging. *J. Vis.* **2006**, *6*, 1057–1067. [[CrossRef](#)] [[PubMed](#)]
4. Garner, L.F.; Yap, M.K. Changes in ocular dimensions and refraction with accommodation. *Ophthalmic Physiol. Opt.* **1997**, *17*, 12–17. [[CrossRef](#)] [[PubMed](#)]
5. Kirschkamp, T.; Dunne, M.; Barry, J.C. Phakometric measurement of ocular surface radii of curvature, axial separations and alignment in relaxed and accommodated human eyes. *Ophthalmic Physiol. Opt.* **2004**, *24*, 65–73. [[CrossRef](#)] [[PubMed](#)]
6. Ciuffreda, K.J. The Glenn, A. Fry invited lecture. Accommodation to gratings and more naturalistic stimuli. *Optom. Vis. Sci.* **1991**, *68*, 243–260. [[CrossRef](#)] [[PubMed](#)]
7. Glasser, A.; Kaufman, P.L. The mechanism of accommodation in primates. *Ophthalmology* **1999**, *106*, 863–872. [[CrossRef](#)]
8. Strenk, S.A.; Semmlow, J.L.; Strenk, L.M.; Munoz, P.; Gronlund-Jacob, J.; DeMarco, J.K. Age-related changes in human ciliary muscle and lens: A Magnetic Resonance Imaging study. *Investig. Ophthalmol. Vis. Sci.* **1999**, *40*, 1162–1169.
9. Richdale, K.; Sinnott, L.T.; Bullimore, M.A.; Wassenaar, P.A.; Schmalbrock, P.; Kao, C.Y.; Patz, S.; Mutti, D.O.; Glasser, A.; Zadnik, K. Quantification of age-related and per diopter accommodative changes of the lens and ciliary muscle in the emmetropic human eye. *Investig. Ophthalmol. Vis. Sci.* **2013**, *54*, 1095–1105. [[CrossRef](#)] [[PubMed](#)]
10. Richdale, K.; Bullimore, M.A.; Sinnott, L.T.; Zadnik, K. The effect of age, accommodation, and refractive error on the adult human eye. *Optom. Vis. Sci.* **2016**, *93*, 3–11. [[CrossRef](#)] [[PubMed](#)]
11. Kasthurirangan, S.; Markwell, E.L.; Atchison, D.A.; Pope, J.M. MRI study of the changes in crystalline lens shape with accommodation and aging in humans. *J. Vis.* **2011**, *11*, 1–16. [[CrossRef](#)] [[PubMed](#)]
12. Jones, C.E.; Atchison, D.A.; Pope, J.M. Changes in lens dimensions and refractive index with age and accommodation. *Optom. Vis. Sci.* **2007**, *84*, 990–995. [[CrossRef](#)] [[PubMed](#)]
13. Khan, A.; Pope, J.M.; Verkicharla, P.K.; Suheimat, M.; Atchison, D.A. Change in human lens dimensions, lens refractive index distribution and ciliary body ring diameter with accommodation. *Biomed. Opt. Express* **2018**, *9*, 1272–1282. [[CrossRef](#)] [[PubMed](#)]
14. Sheppard, A.L.; Evans, C.J.; Singh, K.D.; Wolffsohn, J.S.; Dunne, M.C.; Davies, L.N. Three-dimensional Magnetic Resonance Imaging of the phakic crystalline lens during accommodation. *Investig. Ophthalmol. Vis. Sci.* **2011**, *52*, 3689–3697. [[CrossRef](#)] [[PubMed](#)]
15. Martinez-Enriquez, E.; Perez-Merino, P.; Velasco-Ocana, M.; Marcos, S. OCT-based full crystalline lens shape change during accommodation in vivo. *Biomed. Opt. Express* **2017**, *8*, 918–933. [[CrossRef](#)] [[PubMed](#)]
16. Shum, P.J.; Ko, L.S.; Ng, C.L.; Lin, S.L. A biometric study of ocular changes during accommodation. *Am. J. Ophthalmol.* **1993**, *115*, 76–81. [[CrossRef](#)]
17. Drexler, W.; Baumgartner, A.; Findl, O.; Hitzenberger, C.K.; Fercher, A.F. Biometric investigation of changes in the anterior eye segment during accommodation. *Vis. Res.* **1997**, *37*, 2789–2800. [[CrossRef](#)]
18. Dubbelman, M.; van der Heijde, G.L.; Weeber, H.A.; Vrensen, G.F. Changes in the internal structure of the human crystalline lens with age and accommodation. *Vis. Res.* **2003**, *43*, 2363–2375. [[CrossRef](#)]
19. Dubbelman, M.; van der Heijde, G.L.; Weeber, H.A. Change in shape of the aging human crystalline lens with accommodation. *Vis. Res.* **2005**, *45*, 117–132. [[CrossRef](#)] [[PubMed](#)]
20. Ostrin, L.; Kasthurirangan, S.; Win-Hall, D.; Glasser, A. Simultaneous measurements of refraction and A-scan biometry during accommodation in humans. *Optom. Vis. Sci.* **2006**, *83*, 657–665. [[CrossRef](#)] [[PubMed](#)]

21. Tsoibatzoglou, A.; Nemeth, G.; Szell, N.; Biro, Z.; Berta, A. Anterior segment changes with age and during accommodation measured with Partial Coherence Interferometry. *J. Cataract. Refract. Surg.* **2007**, *33*, 1597–1601. [[CrossRef](#)] [[PubMed](#)]
22. Read, S.A.; Collins, M.J.; Woodman, E.C.; Cheong, S.H. Axial length changes during accommodation in myopes and emmetropes. *Optom. Vis. Sci.* **2010**, *87*, 656–662. [[CrossRef](#)] [[PubMed](#)]
23. Strenk, S.A.; Strenk, L.M.; Semmlow, J.L.; DeMarco, J.K. Magnetic Resonance Imaging study of the effects of age and accommodation on the human lens cross-sectional area. *Investig. Ophthalmol. Vis. Sci.* **2004**, *45*, 539–545. [[CrossRef](#)]
24. Strenk, S.A.; Strenk, L.M.; Koretz, J.F. The mechanism of presbyopia. *Prog. Retin. Eye Res.* **2005**, *24*, 379–393. [[CrossRef](#)] [[PubMed](#)]
25. Hermans, E.; Dubbelman, M.; van der Heijde, R.; Heethaar, R. The shape of the human lens nucleus with accommodation. *J. Vis.* **2007**, *7*, 1–10. [[CrossRef](#)] [[PubMed](#)]
26. Richdale, K.; Bullimore, M.A.; Zadnik, K. Lens thickness with age and accommodation by Optical Coherence Tomography. *Ophthalmic Physiol. Opt.* **2008**, *28*, 441–447. [[CrossRef](#)] [[PubMed](#)]
27. Doyle, L.; Little, J.A.; Saunders, K.J. Repeatability of OCT lens thickness measures with age and accommodation. *Optom. Vis. Sci.* **2013**, *90*, 1396–1405. [[CrossRef](#)] [[PubMed](#)]
28. Davies, L.N.; Dunne, M.C.; Gibson, G.A.; Wolffsohn, J.S. Vergence analysis reveals the influence of axial distances on accommodation with age and axial ametropia. *Ophthalmic Physiol. Opt.* **2010**, *30*, 371–378. [[CrossRef](#)] [[PubMed](#)]
29. Vilupuru, A.S.; Glasser, A. The relationship between refractive and biometric changes during Edinger-Westphal stimulated accommodation in Rhesus monkeys. *Exp. Eye Res.* **2005**, *80*, 349–360. [[CrossRef](#)] [[PubMed](#)]
30. Storey, J.K.; Rabie, E.P. Ultrasound-A research tool in the study of accommodation. *Ophthalmic Physiol. Opt.* **1983**, *3*, 315–320. [[CrossRef](#)] [[PubMed](#)]
31. Beauchamp, R.; Mitchell, B. Ultrasound measures of vitreous chamber depth during ocular accommodation. *Am. J. Optom. Physiol. Opt.* **1985**, *62*, 523–532. [[CrossRef](#)] [[PubMed](#)]
32. Koretz, J.F.; Bertasso, A.M.; Neider, M.W.; True-Gabelt, B.A.; Kaufman, P.L. Slit-lamp studies of the Rhesus monkey eye: II. Changes in crystalline lens shape, thickness and position during accommodation and aging. *Exp. Eye Res.* **1987**, *45*, 317–326. [[CrossRef](#)]
33. Wendt, M.; Croft, M.A.; McDonald, J.; Kaufman, P.L.; Glasser, A. Lens diameter and thickness as a function of age and pharmacologically stimulated accommodation in rhesus monkeys. *Exp. Eye Res.* **2008**, *86*, 746–752. [[CrossRef](#)] [[PubMed](#)]
34. Van der Heijde, G.L.; Weber, J. Accommodation used to determine ultrasound velocity in the human lens. *Optom. Vis. Sci.* **1989**, *66*, 830–833. [[CrossRef](#)] [[PubMed](#)]
35. Van der Heijde, G.L.; Beers, A.P.; Dubbelman, M. Microfluctuations of steady-state accommodation measured with Ultrasonography. *Ophthalmic Physiol. Opt.* **1996**, *16*, 216–221. [[CrossRef](#)] [[PubMed](#)]
36. Beers, A.P.; van der Heijde, G.L. In vivo determination of the biomechanical properties of the component elements of the accommodation mechanism. *Vis. Res.* **1994**, *34*, 2897–2905. [[CrossRef](#)]
37. Beers, A.P.; van der Heijde, G.L. Presbyopia and velocity of sound in the lens. *Optom. Vis. Sci.* **1994**, *71*, 250–253. [[CrossRef](#)] [[PubMed](#)]
38. Beers, A.P.; van der Heijde, G.L. Age-related changes in the accommodation mechanism. *Optom. Vis. Sci.* **1996**, *73*, 235–242. [[CrossRef](#)] [[PubMed](#)]
39. Croft, M.A.; McDonald, J.P.; Nadkarni, N.V.; Lin, T.L.; Kaufman, P.L. Age-related changes in centripetal ciliary body movement relative to centripetal lens movement in monkeys. *Exp. Eye Res.* **2009**, *89*, 824–832. [[CrossRef](#)] [[PubMed](#)]
40. Croft, M.A.; Nork, T.M.; McDonald, J.P.; Katz, A.; Lutjen-Drecoll, E.; Kaufman, P.L. Accommodative movements of the vitreous membrane, choroid, and sclera in young and presbyopic human and nonhuman primate eyes. *Investig. Ophthalmol. Vis. Sci.* **2013**, *54*, 5049–5058. [[CrossRef](#)] [[PubMed](#)]
41. Croft, M.A.; Heatley, G.; McDonald, J.P.; Katz, A.; Kaufman, P.L. Accommodative movements of the lens/capsule and the strand that extends between the posterior vitreous zonule insertion zone & the lens equator, in relation to the vitreous face and aging. *Ophthalmic Physiol. Opt.* **2016**, *36*, 21–32. [[PubMed](#)]

42. He, L.; Wendt, M.; Glasser, A. Pharmacologically and Edinger-Westphal stimulated accommodation in Rhesus monkeys does not rely on changes in anterior chamber pressure. *Exp. Eye Res.* **2014**, *125*, 244–255. [[CrossRef](#)] [[PubMed](#)]
43. Lutjen-Drecoll, E.; Kaufman, P.L.; Wasielewski, R.; Ting-Li, I.; Croft, M.A. Morphology and accommodative function of the vitreous zonule in human and monkey eyes. *Investig. Ophthalmol. Vis. Sci.* **2010**, *51*, 1554–1564. [[CrossRef](#)] [[PubMed](#)]
44. Brown, N. The change in shape and internal form of the lens of the eye on accommodation. *Exp. Eye Res.* **1973**, *15*, 441–459. [[CrossRef](#)]
45. Dubbelman, M.; van der Heijde, G.L. The shape of the aging human lens: Curvature, equivalent refractive index and the lens paradox. *Vis. Res.* **2001**, *41*, 1867–1877. [[CrossRef](#)]
46. Dubbelman, M.; van der Heijde, G.L.; Weeber, H.A. The thickness of the aging human lens obtained from corrected Scheimpflug images. *Optom. Vis. Sci.* **2001**, *78*, 411–416. [[CrossRef](#)] [[PubMed](#)]
47. Dubbelman, M.; Weeber, H.A.; van der Heijde, R.G.; Volker-Dieben, H.J. Radius and asphericity of the posterior corneal surface determined by corrected Scheimpflug photography. *Acta Ophthalmol. Scand.* **2002**, *80*, 379–383. [[CrossRef](#)] [[PubMed](#)]
48. Mallen, E.A.; Kashyap, P.; Hampson, K.M. Transient axial length change during the accommodation response in young adults. *Investig. Ophthalmol. Vis. Sci.* **2006**, *47*, 1251–1254. [[CrossRef](#)] [[PubMed](#)]
49. Baikoff, G.; Lutun, E.; Ferraz, C.; Wei, J. Static and dynamic analysis of the anterior segment with Optical Coherence Tomography. *J. Cataract. Refract. Surg.* **2004**, *30*, 1843–1850. [[CrossRef](#)] [[PubMed](#)]
50. Baikoff, G.; Lutun, E.; Ferraz, C.; Wei, J. Analysis of the eye's anterior segment with Optical Coherence Tomography. Static and dynamic study. *J. Fr. Ophthalmol.* **2005**, *28*, 343–352. [[CrossRef](#)]
51. Baikoff, G.; Lutun, E.; Wei, J.; Ferraz, C. An in vivo OCT study of human natural accommodation in a 19-year-old albino. *J. Fr. Ophthalmol.* **2005**, *28*, 514–519. [[CrossRef](#)]
52. Goldsmith, J.A.; Li, Y.; Chalita, M.R.; Westphal, V.; Patil, C.A.; Rollins, A.M.; Izatt, J.A.; Huang, D. Anterior chamber width measurement by high-speed Optical Coherence Tomography. *Ophthalmology* **2005**, *112*, 238–244. [[CrossRef](#)] [[PubMed](#)]
53. Lavanya, R.; Teo, L.; Friedman, D.S.; Aung, H.T.; Baskaran, M.; Gao, H.; Alfred, T.; Seah, S.K.; Kashiwagi, K.; Foster, P.J.; et al. Comparison of anterior chamber depth measurements using the IOLMaster, scanning peripheral anterior chamber depth analyser, and anterior segment Optical Coherence Tomography. *Br. J. Ophthalmol.* **2007**, *91*, 1023–1026. [[CrossRef](#)] [[PubMed](#)]
54. Nemeth, G.; Vajas, A.; Tsoibatzoglou, A.; Kolozsvari, B.; Modis, L., Jr.; Berta, A. Assessment and reproducibility of anterior chamber depth measurement with anterior segment Optical Coherence Tomography compared with immersion Ultrasonography. *J. Cataract. Refract. Surg.* **2007**, *33*, 443–447. [[CrossRef](#)] [[PubMed](#)]
55. Leung, C.K.; Li, H.; Weinreb, R.N.; Liu, J.; Cheung, C.Y.; Lai, R.Y.; Pang, C.P.; Lam, D.S. Anterior chamber angle measurement with anterior segment Optical Coherence Tomography: A comparison between slit lamp OCT and Visante OCT. *Investig. Ophthalmol. Vis. Sci.* **2008**, *49*, 3469–3474. [[CrossRef](#)] [[PubMed](#)]
56. Dawczynski, J.; Koenigsdoerffer, E.; Augsten, R.; Strobel, J. Anterior segment Optical Coherence Tomography for evaluation of changes in anterior chamber angle and depth after intraocular lens implantation in eyes with glaucoma. *Eur. J. Ophthalmol.* **2007**, *17*, 363–367. [[CrossRef](#)] [[PubMed](#)]
57. Dang, N.P.; Cottet, L.; Dosso, A.A. Evaluation of the anterior chamber depth after cataract surgery with OCT Visante. *Klin. Monbl. Augenheilkd.* **2008**, *225*, 438–440.
58. Baikoff, G. Anterior segment OCT and phakic intraocular lenses: A perspective. *J. Cataract. Refract. Surg.* **2006**, *32*, 1827–1835. [[CrossRef](#)] [[PubMed](#)]
59. Koivula, A.; Kugelberg, M. Optical Coherence Tomography of the anterior segment in eyes with phakic refractive lenses. *Ophthalmology* **2007**, *114*, 2031–2037. [[CrossRef](#)] [[PubMed](#)]
60. Guell, J.L.; Morral, M.; Gris, O.; Gaytan, J.; Sisquella, M.; Manero, F. Evaluation of Verisyse and Artiflex phakic intraocular lenses during accommodation using Visante optical coherence tomography. *J. Cataract. Refract. Surg.* **2007**, *33*, 1398–1404. [[CrossRef](#)] [[PubMed](#)]
61. Kaiserman, I.; Bahar, I.; Rootman, D.S. Corneal wound malapposition after penetrating keratoplasty: An optical coherence tomography study. *Br. J. Ophthalmol.* **2008**, *92*, 1103–1107. [[CrossRef](#)] [[PubMed](#)]
62. Konstantopoulos, A.; Hossain, P.; Anderson, D.F. Recent advances in ophthalmic anterior segment imaging: A new era for ophthalmic diagnosis? *Br. J. Ophthalmol.* **2007**, *91*, 551–557. [[CrossRef](#)] [[PubMed](#)]

63. Cheng, A.C.; Rao, S.K.; Lau, S.; Leung, C.K.; Lam, D.S. Central corneal thickness measurements by Ultrasound, Orbscan II, and Visante OCT after LASIK for myopia. *J. Refract. Surg.* **2008**, *24*, 361–365. [[PubMed](#)]
64. Bolz, M.; Prinz, A.; Drexler, W.; Findl, O. Linear relationship of refractive and biometric lenticular changes during accommodation in emmetropic and myopic eyes. *Br. J. Ophthalmol.* **2007**, *91*, 360–365. [[CrossRef](#)] [[PubMed](#)]
65. Norrby, S. The Dubbelman Eye Model analysed by ray tracing through aspheric surfaces. *Ophthalmic Physiol. Opt.* **2005**, *25*, 153–161. [[CrossRef](#)] [[PubMed](#)]
66. Davies, L.N.; Mallen, E.A.; Wolffsohn, J.S.; Gilmartin, B. Clinical evaluation of the Shin-Nippon Nvision-K 5001/Grand Seiko WR-5100k autorefractor. *Optom. Vis. Sci.* **2003**, *80*, 320–324. [[CrossRef](#)] [[PubMed](#)]
67. Stark, L.R.; Atchison, D.A. Subject instructions and methods of target presentation in accommodation research. *Investig. Ophthalmol. Vis. Sci.* **1994**, *35*, 528–537.
68. Francis, E.L.; Jiang, B.C.; Owens, D.A.; Tyrrell, R.A. Accommodation and vergence require effort-to-see. *Optom. Vis. Sci.* **2003**, *80*, 467–473. [[CrossRef](#)] [[PubMed](#)]
69. Bailey, M.D.; Sinnott, L.T.; Mutti, D.O. Ciliary body thickness and refractive error in children. *Investig. Ophthalmol. Vis. Sci.* **2008**, *49*, 4353–4360. [[CrossRef](#)] [[PubMed](#)]
70. Armstrong, R. A.; Eperjesi, F.; Gilmartin, B. The application of analysis of variance (ANOVA) to different experimental designs in optometry. *Ophthalmic Physiol. Opt.* **2002**, *22*, 248–256. [[CrossRef](#)] [[PubMed](#)]
71. Faul, F.; Erdfelder, E.; Buchner, A.; Lang, A.G. Statistical power analyses using G\*Power 3.1: tests for correlation and regression analyses. *Behav. Res. Methods* **2009**, *41*, 1149–1160. [[CrossRef](#)] [[PubMed](#)]
72. Dunne, M.C.; Davies, L. N.; Wolffsohn, J.S. Accuracy of cornea and lens biometry using anterior segment optical coherence tomography. *J. Biomed. Opt.* **2007**, *12*. [[CrossRef](#)] [[PubMed](#)]
73. Sebag, J. Anatomy and pathology of the vitreo-retinal interface. *Eye* **1992**, *6*, 541–552. [[CrossRef](#)] [[PubMed](#)]
74. Read, S.A.; Buehren, T.; Collins, M.J. Influence of accommodation on the anterior and posterior cornea. *J. Cataract. Refract. Surg.* **2007**, *33*, 1877–1885. [[CrossRef](#)] [[PubMed](#)]
75. Bayramlar, H.; Sadigov, F.; Yildirim, A. Effect of accommodation on corneal topography. *Cornea* **2013**, *32*, 1251–1254. [[CrossRef](#)] [[PubMed](#)]
76. Ortiz, S.; Pérez-Merino, P.; Gamba, E.; de Castro, A.; Marcos, S. In vivo human crystalline lens topography. *Biomed. Opt. Express* **2012**, *3*, 2471–2488. [[CrossRef](#)] [[PubMed](#)]
77. Garner, L.F.; Smith, G. Changes in equivalent and gradient refractive index of the crystalline lens with accommodation. *Optom. Vis. Sci.* **1997**, *74*, 114–119. [[CrossRef](#)] [[PubMed](#)]
78. Glasser, A.; Campbell, M.C. Biometric, optical and physical changes in the isolated human crystalline lens with age in relation to presbyopia. *Vis. Res.* **1999**, *39*, 1991–2015. [[CrossRef](#)]
79. Borja, D.; Siedlecki, D.; de Castro, A.; Uhlhorn, S.; Ortiz, S.; Arrieta, E.; Parel, J.M.; Marcos, S.; Manns, F. Distortions of the posterior surface in optical coherence tomography images of the isolated crystalline lens: Effect of the lens index gradient. *Biomed. Opt. Express* **2010**, *1*, 1331–1340. [[CrossRef](#)] [[PubMed](#)]
80. Siedlecki, D.; de Castro, A.; Gamba, E.; Ortiz, S.; Borja, D.; Uhlhorn, S.; Manns, F.; Marcos, S.; Parel, J.M. Distortion correction of OCT images of the crystalline lens: Gradient index approach. *Optom. Vis. Sci.* **2012**, *89*, 709–718. [[CrossRef](#)] [[PubMed](#)]
81. Uhlhorn, S.R.; Borja, D.; Manns, F.; Parel, J.M. Refractive index measurement of the isolated crystalline lens using optical coherence tomography. *Vis. Res.* **2008**, *27*, 2732–2738. [[CrossRef](#)] [[PubMed](#)]

